Submission to the *American Mineralogist*

Revised manuscript (after "minor modifications" request)

June 19, 2013

Thermodynamic basis for evolution of apatite in calcified tissues

Sabrina Rollin-Martinet[a,b], Alexandra Navrotsky[c], Eric Champion[b], David Grossin[a], and Christophe Drouet[a,*]

[a]CIRIMAT Carnot Institute, University of Toulouse, UMR 5085 CNRS/INPT/UPS, ENSIACET, 4 allee Emile Monso, 31030 Toulouse cedex 4, France (Corresponding author, E-mail: christophe.drouet@ensiacet.fr

[b]Université de Limoges, CNRS, SPCTS, UMR 7315, Centre Européen de la Céramique, 12 rue Atlantis, 87068 Limoges cedex, France (E-mail: eric.champion@unilim.fr)

[c]Peter A. Rock Thermochemistry Laboratory and NEAT ORU, University of California Davis, 1 Shields Ave., Davis CA 95616 USA (E-mail: anavrotsky@ucdavis.edu)

Main corresponding Author:

Dr. Christophe Drouet
CIRIMAT Carnot Institute
ENSIACET
4 allee Emile Monso
31030 Toulouse cedex 4, France

E-mail: christophe.drouet@ensiacet.fr

Abstract

Bone remodeling and tooth enamel maturation are biological processes which alter the physico-chemical features of biominerals with time. However, although the ubiquity of bone remodeling is clear, why is well crystallized bone mineral systematically replaced by immature nanocrystalline inorganic material? In enamel, a clear evolution is also seen from the first mineral formed during the secretory stage and its mature well crystalline form, which then changes little in the adult tooth. This contribution provides the thermodynamic basis underlying these biological phenomena. We determined, for the first time, the energetics of biomimetic apatites corresponding to an increasing degree of maturation. Our data point out the progressive evolution of the enthalpy ($\Delta H_f°$) and free energy ($\Delta G_f°$) of formation toward more negative values upon maturation. Entropy contributions to $\Delta G_f°$ values remained small compared to enthalpy contributions. $\Delta H_f°$ varied from -12058.9 ± 12.2 to -12771.0 ± 21.4 kJ/mol for maturation times increasing from 20 min to 3 weeks, approaching the value for stoichiometric hydroxyapatite, -13431.0 ± 22.7 kJ/mol. Apatite thermodynamic stability increased as its composition moved toward stoichiometry. These findings imply diminishing aqueous solubility of calcium and phosphate ions as well as decreased surface reactivity. Such thermodynamically-driven maturation is favorable for enamel maturation since this biomineral is intended to resist external aggressions such as contact with acids. In contrast, maintaining a metastable highly reactive and soluble form of apatite is essential to the effective participation of bone as a source of calcium and phosphate for homeostasis. Therefore our data strongly suggest that, far from being trivial, the intrinsic thermodynamic properties of apatite mineral represent a critical driving force for continuous bone remodeling, in contrast to current views favoring a purely biologically driven cycle. These thermodynamic data may prove helpful in other domains relating, for example, to apatite-based biomaterials development or in the field of (geo)microbiology.

1. Introduction

Calcified tissues are complex adaptive biomaterials optimized through evolution to provide a union of inorganic and organic constituents to serve both mechanical and biological functions. In particular, one can underline the sophisticated multi-scale architectures found in tooth enamel and in bone, which control their mechanical and chemical properties (Weiner and Wagner 1998, Gomez-Morales et al. 2013). Along with morphological aspects, the chemical composition, crystal structure and microstructure of such apatitic biominerals are oadapted to their physiological functions. Enamel, for instance, is intended to protect erupted teeth against external aggressions (thermal, mechanical, chemical), and thus requires in its mature state a high degree of chemical and mechanical stability and low aqueous solubility. These conditions are met thanks to a chemical composition and other physico-chemical features for mature enamel close to stoichiometric hydroxyapatite (HA, hexagonal, $P6_3/m$ space group) (Bonar et al. 1991). In contrast, far from being inert, bone acts as an ion reservoir allowing for the continual regulation of mineral ion concentrations in body fluids (homeostasis) (Driessens et al. 1986). Therefore, bone mineral should be relatively soluble and should remain highly reactive. Such an increase in solubility and reactivity relative to well-crystallized stoichiometric hydroxyapatite can be attained through nonstoichiometry (ion vacancies) as well as by nanometric crystal dimensions and a low degree of crystallinity (Grynpas 1976).

Without taking into account the presence of secondary elements, the overall composition of biomimetic apatite can generally be satisfactorily described by formulas such as: $Ca_{10-x}(PO_4)_{6-x}(HPO_4)_x(OH)_{2-x}$ (proposed by Winand 1961) or $Ca_{10-x-Z}(PO_4)_{6-x}(HPO_4)_x(OH)_{2-x-2Z}$ (proposed by Kühl and Nebergall 1963), where x and Z depend on factors such as conditions of formation and/or state of ageing. The presence of carbonate ions is also observed, especially in mature biominerals (Gomez-Morales et al. 2013), whereas significantly lower carbonate amounts are found in immature ones (Rey

et al. 1995). The reactivity of such nanocrystalline apatites is directly connected to specific substructural features: detailed works on such nanocrystalline apatite compounds, mostly based on spectroscopic studies (Roufosse et al. 1984; Rey et al. 1989a; Rey et al. 1990; Lu et al., 2000; Kaflak et al. 2008), reveal the presence of non-apatitic ionic environments located within a calcium phosphate hydrated layer on the surface of the nanocrystals, whether of synthetic or of biological origin (Cazalbou et al. 2004a; Rey et al. 1989b). This type of complex substructure can probably be related to the mode of formation of apatites (Cazalbou et al. 2004b), which enclose a large number of ions per unit formula and for which the kinetics of crystallization is slow.

The surface layer has been shown to be mostly composed of divalent ions (e.g. Ca^{2+}, HPO_4^{2-}…), that are rather labile and can be easily and rapidly exchanged (within a few minutes) by other ions from the surrounding fluid (Eichert et al. 2008). Ion exchange isotherms with Langmuir-like features are generally seen (Drouet et al. 2008). Also, the presence of this layer plays a key role in the adsorption of (bio)molecules (Ouizat et al. 1999), and such adsorption phenomena sometimes involve a simultaneous release of surface ions (Errassifi et al. 2010). The presence of this layer generally leads to amorphous-like features on electron microscopy analyses (Sakhno et al. 2010), and solid state NMR data also distinguish between the less-ordered surface ionic environments and bulk species (Wu et al. 2002; Jager et al. 2006; Kaflak et al. 2008).

The preparation of synthetic analogs to biological apatites – i.e. mimicking at the same time compositional, crystallographic and microstructural features – has been made possible at the laboratory scale using “mild” synthetic conditions, generally through precipitation at room temperature and physiological pH (Rey et al. 1989b; Cazalbou et al. 2004a; Cazalbou et al. 2004b; Drouet et al. 2009). Variations in synthesis protocols, especially modification of temperature, pH and/or maturation time prior to precipitate filtration, significantly alter the structural and chemical characteristics of the nanocrystals (Vandecandelaere et al. 2012). An increase of maturation time (ageing in solution) leads to an increase in mean crystallite dimensions as well as a progressive evolution of the chemical

composition toward the stoichiometry of hydroxyapatite ($Ca_{10}(PO_4)_6(OH)_2$, denoted "HA") (Cazalbou et al. 2004a), much like what is observed *in vivo* for enamel maturation between the initial stages of formation (during the secretory stage by ameloblast cells) and its mature state (Rey et al. 1995; Gomez-Morales et al. 2013). Also, a decrease in surface reactivity, measured either by ion exchange or adsorption, has been noticed for crystals matured for increasing periods of time in an aqueous medium (Ouizat et al. 1999; Eichert et al. 2008). In the case of bone, several works have reported the modification in mineral composition and in the amount of non-apatitic surface species upon ageing, with an increase of the amount of carbonate and a decrease of the HPO_4 content (Kühl and Nebergall 1963; Legros et al. 1987; Rey et al. 1991a; Rey et al. 1995). During this ageing process, some ions of the surface layer are likely to be incorporated into the apatitic core of the nanocrystals and the overall surface area decreases. These changes may then limit ion exchange which plays a key role in physiological pathways (Neuman et al. 1956; Pak et al. 1967; Neuman et al. 1968; Johnson et al. 1970; Fernandez-Gavarron 1978; Neuman and Neuman 1985).

Although apatite nanocrystal maturation/ageing has been the object of much investigation, no quantification of the energetics of biomimetic apatite compounds nor of their ageing can be found in the literature to the best of our knowledge; as only thermodynamic data for stoichiometric coarsely crystalline apatitic compounds are available (Jemal et al. 1995; Jemal 2004; Ben Cherifa and Jemal 2004). The object of this contribution is to investigate the energetic evolution of precipitated biomimetic apatite during ageing, based on solution calorimetric studies coupled with careful characterization and chemical analyses, and to relate the energetics to the behavior of apatite nanocrystal biominerals, linked in particular to enamel maturation and to bone remodeling. This study was carried out on non-carbonated apatites, thus more specifically addressing the first stages of biomineral maturation processes (Rey et al. 1995).

2. Materials and Methods

2.1. Synthesis of nanocrystalline apatite compounds

Biomimetic (non-carbonated) nanocrystalline apatite compounds were prepared by precipitation from mixing aqueous solutions of di-ammonium hydrogenphosphate (0.6 M) and calcium nitrate (0.3 M), at 22 °C and at pH = 7.2 close to the physiological value. The excess of phosphate ions in solution, relative to the formation of hydroxyapatite, provides an internal pH buffer without any additives in the precipitating medium. After rapid mixing (1 min), the precipitates were left to mature (ageing in solution) for different periods of time, namely 20 min, 3 h, 1 day, 3 days, 5 days, 1 week and 3 weeks. Then the precipitates were filtered on Büchner funnel, thoroughly washed with deionized water and freeze-dried (freeze-dryer set to -80 °C, residual pressure 10 mbar).

Stoichiometric HA was prepared following a previously reported protocol (Raynaud et al. 2002). Briefly, the precipitation was carried out under reflux at 90 °C and pH = 8.5 from adding dropwise a solution of di-ammonium phosphate into a solution of calcium nitrate. The synthesis was carried out under argon atmosphere to avoid atmospheric contamination, especially of CO_2. The reactants were used in stoichiometric proportions, in the presence of ammonia for pH stabilization. The mixture was aged for 90 min prior to filtration on Büchner funnel and washing with deionized water. The precipitate was then oven-dried at 80 °C for 24 h and calcined at 1000 °C for 15 h.

β-TCP was obtained by calcining at 900 °C for 16 h some amorphous calcium phosphate (am-$Ca_3(PO_4)_2$) prepared by rapid precipitation from calcium nitrate (0.36 M) and di-ammonium hydrogenphosphate (0.154 M) solutions under strongly alkaline conditions (pH = 10) after the protocol proposed by Heughebaert and Montel (Heughebaert and Montel 1982).

2.2. Characterization techniques

Powder X-ray diffraction (XRD) was performed for crystal structure identification, using a Brüker D8

Advance diffractometer with the monochromatic $CuK_{\alpha 1}$ radiation (λ = 1.5406 Å, step 0.021°). XRD profile fitting was performed using the JANA 2006 software. The crystallite mean length was estimated by applying the Hosemann and Vogel model (Vogel and Hosemann 1970) to the (002) and (004) planes, as this model takes into account the possible existence of non-negligible crystal disorder effects.

Fourier transform infrared (FTIR) was used, in transmission mode, for complementary phase identification. The experiments were carried out on a Perkin Elmer 1600 spectrometer, in the wavenumber range 400-4000 cm^{-1} and at 4 cm^{-1} resolution.

The calcium content of the solids was determined by complexometry with EDTA (Charlot 1974). The relative error is 0.5%. Orthophosphate ionic contents (PO_4^{3-}, HPO_4^{2-}) were measured by colorimetry (λ = 460 nm) based on the yellow phospho-vanado-molybdenum complex $VO_3[P(Mo_3O_{10})_4]$ formed in acidic conditions (Gee and Dietz 1953). Measurements were carried out in quartz holder with an UV-visible Hitachi Instruments U-1100 single beam spectrophotometer. These orthophosphate ion titrations have a relative error of 0.5 %. The amount of the protonated species HPO_4^{2-} ions is derived by comparing titrations carried out before and after calcining the samples at 600 °C for 1 h, which leads to the condensation of HPO_4^{2-} ions into pyrophosphate ions ($P_2O_7^{4-}$) that do not form the yellow complex, as detailed by Gee and Dietz (Gee and Dietz 1953).

The thermal behavior of the differently matured apatites was followed by thermogravimetry (TG) analyses carried out in air on a Setaram SETSYS Evolution apparatus (heating rate 2.5 °C/min, temperature range 20 – 900 °C). Water contents of the starting powders were derived from the weight loss observed in the temperature range 20 – 300 °C.

2.3. High Temperature Oxide Melt Solution Calorimetry

High-temperature drop solution calorimetry was carried out in a Tian-Calvet twin calorimeter, as

described in detail by Navrotsky (Navrotsky 1977, 1997). Drop solution enthalpies were measured by dropping 5 mg pressed pellets of material directly from room temperature, 298 K, into the molten solvent in the calorimeter, 973 K. Sodium molybdate ($3Na_2O \cdot 4MoO_3$) was selected as appropriate solvent for this work based on earlier data (Ushakov et al. 2001) showing that all phosphorus was retained in the melt after dropping P_2O_5 or other phosphate-containing compounds.

Total calorimetric reaction times during calorimetry were in all cases less than 1 h. The shape of the calorimetric peaks was consistent with rapid sample dissolution during the first few minutes of reaction. The end of the reaction was judged by the return of the baseline to its initial value. A minimum of 8 values were obtained for each composition, and uncertainties are two standard deviations from the mean value. During the experiments, air was flushed through the gas space above the melt (~80 mL/min) so as to accelerate the elimination of gases produced (H_2O or CO_2).

3. Results and Discussion

3.1. Characterization

The calcium phosphate apatite samples prepared in this study with varying maturation times (**Table 1**) were characterized by complementary techniques. TEM observations showed that all prepared samples exhibited a platelet morphology (see typical example of the 1-day maturation sample on **Figure 1**). This plate-like morphology is characteristic of that of bone apatite (morphological biomimetism) as reported in the literature (Johansen and Parks 1960). Powder XRD patterns exhibited diffraction peaks that could all be attributed to a hydroxyapatite-like phase (hexagonal, $P6_3/m$ space group, PDF card 09-0432) as indicated in **Figure 2**. The samples are characterized by a low degree of crystallinity, as for natural bone mineral (Gomez-Morales et al. 2013) or immature enamel crystals (Rey et al. 1995; Gomez-Morales et al. 2013). The crystallinity of these synthetic materials progressively increases upon maturation in accordance with previous data (Neuman et al. 1956; Vandecandelaere et al. 2013). This

increased degree of crystallinity is indicated by the better resolution of the XRD patterns, which is especially visible for peaks (002), (004) and (310) in the 2θ = 28-36° range. XRD peak broadening analysis, using the Hosemann and Vogel model (Vogel and Hosemann 1970), led to the evaluation of mean crystallite dimensions. The longest mean crystallite dimension is accessible from analysis of the (002) and (004) peaks and increases from *ca.* 12 to 27 nm for maturation times ranging from 20 min to 3 weeks, thus confirming the nanocrystalline character of these samples.

FTIR analyses further confirm the apatitic nature of the samples (**Figure 3a**). Detailed observation of the spectra reveal, as expected from previous studies (Rey et al. 2007a; Rey et al. 2007b), the presence of non-apatitic contributions, especially in the ν_4PO_4 vibration region (400-800 cm^{-1}) and more specifically at 535 cm^{-1} (non-apatitic HPO_4^{2-} ions) and 617 cm^{-1} (non-apatitic PO_4^{3-}). For more mature samples, the libration band of apatitic OH^- at 631 cm^{-1} becomes visible (see **Figure 3b**, illustrating an apatite matured for 1 week). The presence of non-apatitic contributions substantiates again the biomimetic character of these apatite compounds (Eichert et al. 2008), and it stresses their departure from the structure and composition of coarse hydroxyapatite "reference" material.

Calcium and phosphate titrations along with thermal analyses and the condition of electroneutrality enabled the determination of the contents of each ionic species and water in every sample produced with increasing maturation times. The determination of HPO_4/PO_4 relative amounts is made possible for such apatite samples due to the absence of carbonate ions, therefore enabling one to determine accurate chemical compositions needed for calorimetric evaluations. Indeed, the HPO_4/PO_4 balance is generally drawn from orthophosphate titration, by comparing results obtained before and after heating the samples at 600 °C (which decomposes HPO_4^{2-} into non-titrable pyrophosphates $P_2O_7^{4-}$), while carbonate ions may interfere with these titration methods by partially reacting with HPO_4^{2-} ions through reactions such as $CO_3^{2-} + 2HPO_4^{2-} \rightarrow CO_2 + 2PO_4^{3-} + H_2O$ (Eichert et al. 2008).

The water content has been assessed from the measured weight loss observed by thermogravimetric

analyses between 20 and 300 °C (see Supplementary Figure AR1) as this range corresponds to the release of such associated water molecules from apatite nanocrystals (Banu 2005). The chemical composition of the samples is reported in **Table 1**. The calcium and hydroxyl contents increase with maturation time, while the HPO_4^{2-} content decreases. These variations produce a progressive evolution of the chemical composition of the samples toward the stoichiometry of hydroxyapatite. This evolution can also be monitored by following the Ca/P mole ratio, which increases here from 1.42 to 1.54 (± 0.02). The amount of associated water molecules also decreases as ageing in solution progresses. These trends suggest the progressive disappearance of the hydrated non-apatitic surface layer from the nanocrystals.

Although the chemical formula $Ca_{10-x}(PO_4)_{6-x}(HPO_4)_x(OH)_{2-x}$ is often used to describe nonstoichiometric apatites, it shows some limitations when applied to the current analytical data, especially for short maturation times. In contrast the formula proposed by Kühl and Nebergall 1963, $Ca_{10-x-Z}(PO_4)_{6-x}(HPO_4)_x(OH)_{2-x-2Z}$, involving lower calcium and hydroxide contents, satisfactorily describes the overall chemical composition of the biomimetic apatite phases prepared in this work, and the values of Z are also indicated in **Table 1**. Z was indeed found to become significant for the most immature samples. Taking into account the presence of « n » moles of water per unit formula in the freeze-dried samples, the complete chemical formula thus becomes: $Ca_{10-x-Z}(PO_4)_{6-x}(HPO_4)_x(OH)_{2-x-2Z} \cdot nH_2O$.

3.2. Enthalpies of formation

The determination of the enthalpy of formation from the oxides of these apatites ($\Delta H_{f,oxides}$) from measured enthalpies of drop solution (ΔH_{ds}) requires the application of a thermodynamic cycle, indicated in **Table 2**. This cycle uses the experimental value of ΔH_{ds} measured for each hydrated apatite corresponding to various maturation stages, as well as the enthalpies of drop solution of

calcium carbonate $CaCO_3$ (calcite) and phosphorus oxide P_2O_5. The latter was determined previously by Ushakov et al. 2001. Calcium carbonate was preferred to calcium oxide in this study taking into account the difficulty to keep anhydrous CaO which has a tendency to partially transform into calcium hydroxide. The enthalpies of formation of the apatites from the elements, $\Delta H_f°$, can then be calculated by adding the appropriate literature values of enthalpies of formation of the binary oxides from their elements. The application of this cycle to reference compounds, namely β-tricalcium phosphate (β-TCP) and stoichiometric hydroxyapatite (**Table**), led to $\Delta H_f°$ values of -4090.2 ± 10.6 kJ/mol and -13431.0 ± 22.7 kJ/mol respectively. These numbers are in good agreement (within ~ 0.7 %) with values reported in the literature (Robie and Hemingway 1995) (-4120.8 ± 5.0 kJ/mol and -13477.0 ± 10.0 kJ/mol respectively, the latter value being expressed for the unit formula $Ca_{10}(PO_4)_6(OH)_2$ rather than $Ca_5(PO_4)_3OH$)), thus validating this cycle and measurements.

The application of the cycle then leads (**Table**) to the evaluation of the standard enthalpies of formation of the apatite samples as prepared (hydrated) as well as those of the apatite phases themselves (anhydrous). As indicated in **Table 2**, the latter were obtained by considering hydration water molecules as thermodynamically equivalent to liquid water, as is often the case for hydrated phases in which H_2O is not tightly bound and can be released below 300 ^oC (Drouet and Navrotsky 2003).

The enthalpy values thus obtained, either relative to the elements or to the oxides, become more negative (exothermic) as maturation progresses. $\Delta H_f°$ varies from -12058.9 ± 12.2 to -12771.0 ± 21.4 kJ/mol for maturation times increasing from 20 min to 3 weeks (**Figure 4a**), thus approaching the value for stoichiometric HA, i.e. -13431.0 ± 22.7 kJ/mol. The $\Delta H_f° = f(t)$ curve follows a monotonic, nearly exponential trend with faster changes during the first 3 days of ageing and slower progression beyond this stage. This trend is then found to parallel the evolutions (in the opposite direction) of the Ca^{2+} and OH^- ion contents of the maturing apatite phases (see Supplementary Figure AR2). Based on

these findings, the enthalpy of formation of a nanocrystalline apatite phase appears to be direcly related to its calcium and hydroxide contents. Indeed, the plot of $\Delta H_f°$ versus Ca^{2+} or OH^- ion content shows roughly linear variations (see Supplementary Figure AR3), with fit parameters taking into account the cumulated experimental uncertainties (R^2 = 0.886 and 0.937 respectively). Since the calcium content can be determined easily by techniques such as EDTA complexometry, ICP-AES or atomic absorption spectroscopy, and is often reported in literature studies (as opposed to the hydroxide content which is less easily accessible) we report here specifically the equation found for the linear fit obtained versus the apatite calcium content: $\Delta H_f°$(apatite) = -903.8 * [Ca^{2+} content] - 4426.7, in kJ/mol, and the relative error on $\Delta H_f°$(apatite) can be estimated to be 1.0 % (see **Figure 4b**). These findings thus allow us to unveil, for the first time quantitatively, the direct correlation between the energetics of formation of biomimetic apatites and their ionic contents. Since the amount of calcium is directly linked to the number of cationic vacancies, and similarly the hydroxide content to the amount of anionic vacancies, $\Delta H_f°$ is found to fundamentally depend on the apatite maturation state: the system gets more energetically favorable (more exothermic $\Delta H_f°$) as there are fewer crystal "defects" in the structure. The linear variation of enthalpy with Ca^{2+} or OH^- contents also supports the fact that this trend is rather independent on the distribution of the calcium ions between the surface hydrated layer and the apatitic core: it thus allows one to extend the use of this prevision trend to other synthesis scenarios leading to nanocrystalline apatites as final product. It should be noted that the contribution of the non-apatitic chemical environments to the energetics cannot at present be separated from the overall energetic trend. Finally, these findings provide weak evidence that clustering or ordering of such defects does not occur with major energetic consequences.

3.3. Entropies and Gibbs free energies

Entropy values for nonstoichiometric nanocrystalline apatites are not accessible from the literature.

Data reported for well-crystallized stoichiometric apatitic compounds such as hydroxy-, fluor- and chlor-apatites are on the contrary available (Jemal et al. 1995; Jemal 2004; Ben Cherifa and Jemal 2004), and a calculation reveals that, in all cases, the entropy contributions of $T \cdot \Delta S_f°$ represent only a minor proportion of the Gibbs free energy of formation $\Delta G_f° = \Delta H_f° - T \cdot \Delta S_f°$ (of the order of 6 %, see Supplementary Figure AR4) compared to the enthalpy contribution $\Delta H_f°$. Therefore the relative stability of such compounds, which are theoretically assessed by comparing $\Delta G_f°$ values, can also be reached in a more direct way by comparing the enthalpies of formation accessed by calorimetry. The data reported in **Figure 4a** therefore suggest that the relative stability of biomimetic apatites increases as maturation progresses, evolving toward the level of stoichiometric hydroxyapatite (without reaching it though).

We obtain a better estimate of the entropy of nanocrystalline apatites by considering the following reaction:

$$(9\text{-}x)\ CaO_{(s,\,298)} + 3\ P_2O_{5(s,\,298)} + (1\text{-}Z)\ Ca(OH)_{2(s,\,298)} \rightarrow Ca_{10\text{-}x\text{-}Z}(PO_4)_{6\text{-}x}(HPO_4)_x(OH)_{2\text{-}x\text{-}2Z(s,\,298)} \quad \text{(Eq. 1)}$$

Since this reaction only involves solid phases, the corresponding entropy change, $\Delta S°_{react}$, is expected to be close to zero. Considering $\Delta S°_{react} = 0$, T = 298 K and entropy values for CaO, P_2O_5 and $Ca(OH)_2$ from thermodynamic databases (Robie and Hemingway 1995), this reaction leads for stoichiometric HA (x = Z = 0) to the standard entropy S°(HA) = 769.5 J/(mol.K). This value is in reasonable agreement (within 1.5 %) with the value 780.8 J/(mol.K) reported in the literature (Robie and Hemingway 1995) (expressed for the unit formula $Ca_{10}(PO_4)_6(OH)_2$) thus supporting this estimation method. In a similar way, the entropy S° of each nanocrystalline apatite from this work was evaluated, as well as the corresponding standard entropy of formation from the elements $\Delta S_f°$ (**Table**

330 **4**). The Gibbs free energies of formation $\Delta G_f°$ could then also be derived, at 298 K, from the $\Delta H_f°$ and
331 $\Delta S_f°$ values. These data show again that the entropy contributions to the $\Delta G_f°$ values are small
332 compared to enthalpy contributions, and that the Gibbs free energy becomes more negative (favorable)
333 as the system gets more mature (**Figure 4a**). This conclusion probably still holds even if one adds the
334 contribution of a possible configurational entropy resulting from the location of defects in the
335 structure, but this contribution cannot be calculated accurately. Note that entropy contributions may
336 presumably also be approximated using computational methods. However, such calculations would
337 require good knowledge of stuctural features, while the exact location of ions contained in the hydrated
338 layer on such biomimetic apatites is still essentially undertermined.

339 A major variation of $\Delta G_f°$ similar to that in $\Delta H_f°$ is found during the first days of maturation in
340 solution, while the decrease in $\Delta G_f°$ becomes less pronounced beyond a few days. A plot of $\Delta G_f°$
341 versus calcium content again leads to a linear trend (see Supplementary Figure AR3), corresponding to
342 the equation $\Delta G_f°$(apatite) = -843.6 * [Ca^{2+} content] – 4204.5 (in kJ/mol, R^2 = 0.880, relative error
343 estimated to 1.1 %). This equation then allows one to draw predictive estimates of the value of $\Delta G_f°$
344 for other calcium phosphate nanocrystalline apatites, based on the determination of their calcium
345 content.

346

347 3.4. Apatite maturation energetics

348 It is desirable to estimate the variation in free energy of maturation $\Delta G_{maturation}(i \rightarrow f)$, corresponding
349 to the maturation process in solution transforming an apatite from an initial maturation stage « i » to a
350 more advanced stage « f ». To this aim, it is necessary to take into account the thermodynamic data for
351 the aqueous ions incorporated or released during this maturation process in solution. This task is
352 however more difficult as it may appear at first sight. Indeed, the maturation process is a complex
353 phenomenon where not only the chemical composition evolves towards stoichiometry, but also where

secondary reactions such as dissolution-reprecipitation may play a role. However, the global change in chemical composition during maturation can probably be considered as a dominant phenomenon, since the overall ion content can significantly change upon maturation as illustrated by **Table 1**, which is bound to quantitatively impact the compounds thermodynamic properties.

Considering the simplified scenario where only the global change in apatite composition is taken into account, it is possible to determine in particular the sign of $\Delta G_{maturation}(i \rightarrow f)$ based on a modeled maturation reaction. The increase in Ca/P ratio that accompanies the observed evolution toward stoichiometry could theoretically either be explained by an additional incorporation of Ca^{2+} ions (increase of numerator) or by a release of phosphate ions in the medium (decrease of denominator), or both. However, the concentration of free calcium ions in solution is likely to be extremely low due to the large excess of phosphate ions in the synthesis medium or to the presence of numerous calcium-complexing entities in body fluids *in vivo* (phosphates, carbonates and protein ionic species). Therefore, the possibility to incorporate additional Ca^{2+} ions from the solution appears unlikely. In contrast, the release of phosphate ions from the solid to the solution appears much more probable, especially as a protonated form which is stable under physiological pH. Since phosphate ions from the non-apatitic surface layer are mostly protonated as HPO_4^{2-}, while the amount of HPO_4^{2-} in the solid decreases upon maturation (in both synthetic and biological apatites) (Rey et al. 1991b; Cazalbou et al. 2004a) in favor of non-protonated PO_4^{3-}, the release of phosphate as $H_2PO_4^-$ appears as the most probable route, which may be described by the following scheme, involving proton hopping between two surface HPO_4^{2-} ions:

$$2\,HPO_4^{2-}{}_{(solid)} \rightarrow H_2PO_4^-{}_{(released\ in\ the\ solution)} + PO_4^{3-}{}_{(solid)} \quad \text{(Eq. 2)}$$

Since this departure of anionic $H_2PO_4^-$ ions from the solid would lead to a decrease in negative

charges, it has to be compensated by a simultaneous incorporation of OH^- ions. This was indeed found experimentally by the increased hydroxylation of apatites upon maturation (**Table 1**). In this context, the global reaction scheme describing the change in composition during the maturation process may probably be written as:

$$\boxed{\textit{Apatite in state « i »}} + \delta_1\, H_2O_{(liq)} \rightarrow \boxed{\textit{Apatite in state “f”}} + \delta_2\, H_2PO_4^-{}_{(aq)} + \delta_3\, H^+_{(aq)} \quad \text{(Eq. 3)}$$

where the chemical species $H_2O_{(liq)}$ and $H^+(aq)$ have been preferred to the direct involvement of $OH^-_{(aq)}$ ions, due to the neutral pH where such maturations were carried out.

The variation in Gibbs free energy accompanying this reaction can be written as $\Delta G_{maturation}(i \rightarrow f) = \Delta G°_{maturation}(i \rightarrow f) + RT * \ln(K)$ where K, the equilibrium constant, is given by the activity product: $(H_2PO_4^-{}_{(aq)})^{\delta 2} * (H^+_{(aq)})^{\delta 3}$. Based on the data in Table 4 and on thermodynamic data (Wagman et al. 1982; Robie and Hemingway 1995) for $H_2O_{(liq)}$ and $H_2PO_4^-{}_{(aq)}$, the values of $\Delta G°_{maturation}(i \rightarrow f)$ were calculated at 298 K for various maturation stages « f » relative to the maturation of 20 min taken as reference (initial state « i »). Also, under physiological conditions (considering pH = 7.4 and $(H_2PO_4^-) \cong 10^{-4}$ M), the values of the RT * ln(K) term for each sample were determined. The obtained values of $\Delta G_{maturation}$ (at 298 K) are plotted in **Figure 5**. The dispersion of the points is probably linked to the simplistic scenario considered here, not taking into account secondary surface reaction in particular. Interestingly, the value of $\Delta G_{maturation}$ is found to be negative in all cases, ranging from 0 to -117 ± 23 kJ/mol, with the most negative value corresponding to evolution toward coarse stoichiometric HA (corresponding to -185 ± 15 kJ/mol). These findings give a quantitative background for biomimetic calcium phosphate apatite ageing (studied here on synthetic samples over a period of 3 weeks maturation).

The spontaneous character of this maturation process can thus be considered as a thermodynamic

driving force explaining the inexorable evolution of nonstoichiometric apatite nanocrystals (e.g. found in immature enamel and in young bone) toward more stable states. Such states are characterized by 1) a composition closer to stoichiometry and 2) an associated decrease in surface reactivity and solubility. This stabilization (in terms of both thermodynamics and kinetics) is advantageous in the case of enamel maturation, taking into account the final functions of this biomineral *in vivo* (i.e. resistance to external aggressions of various nature including chemical). On the contrary, it is not beneficial in the case of bone which needs to remain relatively soluble and reactive (i.e. able to exchange ions with surrounding fluids, and/or to undergo dissolution/reprecipitation phenomena upon remodeling). Our findings thus suggest that bone remodeling has a strong thermodynamic basis. Indeed, according to our data, the metastable apatite composing newly-formed bone matter is thermodynamically driven to inevitably transform into a more stable, less soluble and less reactive state, with lower surface area, minimized non-apatitic surface layer, and fewer reactive surface sites. Such lowered surface reactivity was for example observed in model experiments run on synthetic nanocrystalline apatite and on chicken bone (Cazalbou et al. 2004a).

Thus the maturation of bone apatite crystals with time is bound to lead to limited capability in body fluids homeostasis. Therefore, the above-quantified thermodynamic *driving force* (negative $\Delta G_{maturation}$) along which reactive but immature apatite nanocrystals evolve toward more mature but less reactive states could be seen as a physical-chemical (rather than purely biological) basis explaining the need for bone to be regularly remodeled. Then, such remodeling does not only allow skeletal growth from infancy to adulthood as well as self-repair after bone injury (healing of bone tissue microfractures linked to pathological or traumatic events), but it is a "necessity" in view of conserving highly-reactive bone biomineral crystals capable of playing their role in homeostasis (e.g. as a participation in the stabilization of calcium, magnesium, strontium, phosphate concentrations in body fluids). Bone remodeling, which "resets" the maturation process, at the biological cost of the

energy and nutrients required for it, is thus favorable and necessary to the organism.

In addition to enabling the estimation of $\Delta G_{maturation}$, the determination of free energies of formation $\Delta G_f°$ for such apatite compounds can be used for other thermodynamic calculations. One obvious other example concerns the evaluation of the solubility product of such biomimetic apatites as a function of their maturation state. The question of solubility is indeed relevant when dealing with enamel formation or bone remodeling processes.. In the case of hydroxyapatite, the dissolution equilibrium can be described by the reaction:

$$Ca_{10}(PO_4)_6(OH)_2 + 2\ H^+_{(aq)} \leftrightarrow 10\ Ca^{2+}_{(aq)} + 6\ PO_4^{3-}{}_{(aq)} + 2\ H_2O_{(liq)} \quad \text{(Eq. 4)}$$

The variation of free energy $\Delta G°_{disso}$ accompanying this reaction is linked to the solubility product K_{sp} by the equation:

$$\Delta G°_{disso} = -\ 2.303 * RT\ * \log(K_{sp}) = 2.303 * RT * pK_{sp} \quad \text{(Eq. 5)}$$

Considering the experimental compositions found in this work, the strict application of this equation at 298 K leads to pK_{sp} values ranging from 96 to 113 (see details in Supplementary Figure AR5). As a general tendency, these calculations suggest that apatite solubility decreases as maturation progresses, tending toward the value for stoichiometric HA (McDowell et al. 1977) (pK_{sp}(HA) = 117). However, several literature studies (Hsu et al. 1994; Baig et al. 1996; Chhettry et al. 1999) have pointed out noticeable differences between the *apparent* solubility of nonstoichiometric calcium phosphate apatites and their *theoretical* value, despite long periods of stabilization in solution, thus showing that the system did not reach the true thermodynamic equilibrium. This phenomenon depicts a situation where dissolution (relatively rapid at first) has essentially stopped and where nucleation/growth processes are

not discernable, over the temporal scale of the experiments. Also the non-constancy of the solubility product for such compounds was unveiled by these studies, as it was found to depend on the fraction of mineral dissolved. This behavior, referred to as Metastable Equilibrium of Solubility (MES), was then found to be related to the existence of microstrains (Higuchi et al. 1984) within the constitutive non-ideal crystals. Nanocrystalline biological and biomimetic apatites exhibit a non-homogeneous chemical composition as the nanocrystals are constituted of an apatitic core surrounded by a non-apatitic surface layer. In these conditions, the observation of altered apparent solubilities – as compared to theoretical values – is rather unsurprising. Due to the incongruence of the dissolution of such nanocrystalline compounds, it should be kept in mind that such pK_{sp} values drawn from $\Delta G°_{disso}$ may only be considered for pointing out the decreasing solubility of biomimetic apatites upon ageing. These pK_{sp} values should however be considered with caution for determining precise calcium and phosphate concentrations in surrounding solutions: for this purpose, experimental solubility tests remain the best approach.

3.5. Implications

The inexorable evolution of immature apatite crystals with time is advantageous in the case of enamel where increased stability and lower solubility are beneficial to the "protection" functionality of this biomineral. In contrast, a similar thermodynamically-driven evolution of apatite is deleterious for bone mineral which plays a key role in the regulation of body fluid ionic concentrations *in vivo* through homeostasis. These results strongly suggest that bone remodeling could be seen as a thermodynamic necessity to eliminate the "too stable" and poorly bioactive aged apatite crystals in favor of the neo-formation of immature, less stable, and highly reactive nanocrystals. The time-dependent evolution of apatite-based calcified tissues such as bone or enamel could thus be dictated – at least in great part – by a thermodynamic driving force, despite the current emphasis on a mostly

biologically driven process. Our data strongly support this new interpretation, with a major role played by mineral thermodynamics.

Beside implications of these thermodynamic data for solubility behavior of nanocrystalline biomimetic apatites, these findings are bound to find other implications. In the domain of ectopic (abnormal or untypical) calcifications, several mineral compounds may be observed *in vivo* (e.g. apatite, pyrophosphate, whitlockite, struvite). Specific reasons for their formation are not yet clearly determined. Yet, thermodynamic stabilities are probably involved in the persistence or transformations of such ectopic mineralizations. Biomaterials for bone replacement based on nanocrystalline apatites show great promise due to their high surface reactivity. However any synthesis or post-synthesis step (e.g. sterilization) which may involve humid conditions and/or heating should be considered cautiously and with good understanding of nanocrystallie apatite physic-chemistry, since further evolution of the apatite and/or phase transformations may then come into play. Finally, thermodynamic data on such calcium phosphate systems may prove useful in other domains such as (geo)microbiology (e.g. calcifications occurring inside eukaryotic cells) (Raven and Knoll 2010) or link to the evolution of life on Earth (e.g. evolution from carbonate-based shells to phosphate-based skeletons).

Acknowledgements:

The authors thank the French Agence Nationale de la Recherche (ANR) for funding in the scope of the NanoBiocer program (ANR-07-BLAN-0373), as well as the Institut National Polytechnique de Toulouse (INPT) and the France Berkeley Fund (FBF) for co-funding.

The authors also thank O. Trofymluk, K. Lilova and A. V. Radha for experimental support.

References

Baig, A.A., Fox, J.L., Hsu, J., Wang, Z.R., Otsuka, M., Higuchi, W.I., and LeGeros, R.Z. (1996) Effect of carbonate content and crystallinity on the metastable equilibrium solubility behavior of carbonated apatites. Journal of Colloid and Interface Science, 179(2), 608-617.

Banu, M. (2005), Ph.D. Institut National Polytechnique de Toulouse (INPT), Toulouse, France.

Ben Cherifa, A., and Jemal, M. (2004) Enthalpy of Formation and Mixing of Calcium-Cadmium Phosphoapatites. Phosph. Res. Bull, 15, 113-118.

Bonar, L.C., Shimizu, M., Roberts, J.E., Griffin, R.G., and Glimcher, M.J. (1991) Structural and composition studies on the mineral of newly formed dental enamel – A chemical, X-ray diffraction, and p-31 and proton nuclear magnetic resonance study. Journal of Bone and Mineral Research, 6(11), 1167-1176.

Cazalbou, S., Combes, C., Eichert, D., Rey, C., and Glimcher, M.J. (2004a) Poorly crystalline apatites: evolution and maturation in vitro and in vivo. Journal of Bone and Mineral Metabolism, 22(4), 310-317.

Cazalbou, S., Eichert, D., Drouet, C., Combes, C., and Rey, C. (2004b) Biological mineralisations based on calcium phosphate. Comptes Rendus Palevol, 3(6-7), 563-572.

Charlot, G. (1974). Chimie Analytique Quantitative, 2. Masson, Paris.

Chhettry, A., Wang, Z.R., Hsu, J., Fox, J.L., Baig, A.A., Barry, A.M., Zhuang, H., Otsuka, M., and Higuchi, W.I. (1999) Metastable equilibrium solubility distribution of carbonated apatite as a function of solution composition. Journal of Colloid and Interface Science, 218(1), 57-67.

Driessens, F.C.M., Vandijk, J.W.E., and Verbeeck, R.M.H. (1986) The role of bone mineral in calcium and phosphate homeostasis. Bulletin Des Societes Chimiques Belges, 95(5-6), 337-342.

Drouet, C., Bosc, F., Banu, M., Largeot, C., Combes, C., Dechambre, C., Estournes, C., Raimbeaux, G., and Rey, C. (2009) Nanocrystalline apatites: From powders to biomaterials. Powder Technology, 190(1-2), 118-122.

521 Drouet, C., Carayon, M., Combes, C., and Rey, C. (2008) Surface enrichment of biomimetic apatites with
522 biologically-active ions Mg^{2+} and Sr^{2+}: A preamble to the activation of bone repair materials. Materials
523 Science and Engineering C, 28(8), 1544-1550.
524 Drouet, C., and Navrotsky, A. (2003) Synthesis, characterization, and thermochemistry of K-Na-H3O jarosites.
525 Geochimica et Cosmochimica Acta, 67(11), 2063-2076.
526 Eichert, D., Drouet, C., Sfihi, H., Rey, C., Combes, C. (2008) Book Chapter: Nanocrystalline apatite based
527 biomaterials: synthesis, processing and characterization. Book: Biomaterials Research Advances, p. 93-
528 143.
529 Errassifi, F., Menbaoui, A., Autefage, H., Benaziz, L., Ouizat, S., Santran, V., Sarda, S., Lebugle, A., Combes, C.,
530 Barroug, A., Sfihi, H., and Rey, C. (2010) Adsorption on apatitic calcium phosphates: applications to
531 drug delivery. Advances in Bioceramics and Biotechnologies, 218, 159-174.
532 Fernandez-Gavarron, F. (1978) The dynamic equilibrium of calcium. In A.P. E. Pina, V. Chagoya de Sanchez, Ed.
533 Temas Bioquim. Actual., p. 41-67. Univ. Nac. Auton. Mexico, Mexico City.
534 Gee, A., and Dietz, V.R. (1953) Determination of phosphate by differential spectrophotometry. Ann. Chem., 25,
535 1320-1324.
536 Grynpas, M. (1976) Crystallinity of bone mineral. Journal of Materials Science, 11(9), 1691-1696.
537 Gómez-Morales, J., Iafisco, M., Delgado-López, J.M., Sarda, S., and Drouet, C. (2013) Progress on the
538 preparation of nanocrystalline apatites and surface characterization: Overview of fundamental and
539 applied aspects. Progress in Crystal Growth and Characterization of Materials, 59, 1-46.
540 Heughebaert, J.C., and Montel, G. (1982) Conversion of amorphous tricalcium phosphate into apatitic
541 tricalcium phosphate. Calcified Tissue International, 34, S103-S108.
542 Higuchi, R., Bowman, B., Freiberger, M., Ryder, O.A., and Wilson, A.C. (1984) DNA-sequences from the Quagga,
543 an extinct member of the horse family. Nature, 312(5991).

544 Hsu, J., Fox, J.L., Higuchi, W.I., Powell, G.L., Otsuka, M., Baig, A., and Legeros, R.Z. (1994) Metastable
545 equilibrium solubility behavior of carbonated apatites. Journal of Colloid and Interface Science, 167(2),
546 414-423.
547 Jager, C., Welzel, T., Meyer-Zaika, W., and Epple, M. (2006) A solid-state NMR investigation of the structure of
548 nanocrystalline hydroxyapatite. Magnetic Resonance in Chemistry, 44(6).
549 Jemal, M. (2004) Thermochemistry and Relative Stability of Apatite Phosphates. Phosph. Res. Bull, 15, 119-124.
550 Jemal, M., Bencherifa, A., Khattech, I., and Ntahomvukiye, I. (1995) Standard enthalpies of formation and
551 mixing of hydroxyapatites and fluorapatites. Thermochimica Acta, 259(1), 13-21.
552 Johansen, E., and Parks, H.F. (1960) Electron microscopic observations on the 3 dimensional morphology of
553 apatite crystallites of human dentine and bone. Journal of Biophysical and Biochemical Cytology, 7(4),
554 743-&.
555 Johnson, A.R., Armstrong, W.D., and Singer, L. (1970) The exchangeability of calcium and strontium of bone in
556 vitro. Calcified tissue research, 6(2), 103-12.
557 Kaflak, A., and Kolodziejski, W. (2008) Kinetics H-1 -> P-31 NMR cross-polarization in bone apatite and its
558 mineral standards. Magnetic Resonance in Chemistry, 46(4), 335-341.
559 Kühl, G., and Nebergall, W.H. (1963) Hydrogenphosphateapatite und carbonatapatite. Z. Anorg. Allg. Chem.,
560 324, 313-320.
561 Legros, R., Balmain, N., and Bonel, G. (1987) Age-related changes in mineral of rat and bovine cortical bone.
562 Calcified Tissue International, 41(3), 137-144.
563 Lu, H.B., Campbell, C.T., Graham, D.J., and Ratner, B.D. (2000) Surface characterization of hydroxyapatite and
564 related calcium phosphates by XPS and TOF-SIMS. Analytical Chemistry, 72(13), 2886-2894.
565 Mc Dowell, H., Gregory, T.M., and Brown, W.E. (1977) J. Res. Natl. Bur. Stand., 81A, 273-281.
566 Navrotsky, A. (1977) Progress and new directions in high-temperature calorimetry. Physics and Chemistry of
567 Minerals, 2(1-2), 89-104.

-. (1997) Progress and new directions in high temperature calorimetry revisited. Physics and Chemistry of Minerals, 24(3), 222-241.

Neuman, W.F., and Neuman, M.W. (1985) Shika Kiso Igakkai Zasshi, 24, 272-281.

Neuman, W.F., Terepka, A.R., Canas, F., and Triffitt, J.T. (1968) The cycling concept of exchange in bone. Calcified tissue research, 2(3), 262-70.

Neuman, W.F., Toribara, T.Y., and Mulryan, B.J. (1956) The surface chemistry of bone. 9. Carbonate-phosphate exchange. J. Am. Chem. Soc., 78, 4263-4266.

Ouizat, S., Barroug, A., Legrouri, A., and Rey, C. (1999) Adsorption of bovine serum albumin on poorly crystalline apatite: Influence of maturation. Materials Research Bulletin, 34(14-15), 2279-2289.

Pak, C.Y.C., and Bartter, F.C. (1967) Ionic interaction with bone mineral. I. Evidence for an isoionic calcium exchange with hydroxyapatite. Biochim. Biophys. Acta, 141, 401-409.

Raven, J.A., and Knoll, A.H. (2010) Non-Skeletal Biomineralization by Eukaryotes: Matters of Moment and Gravity. Geomicrobiology Journal, 27(6-7), 572-584.

Raynaud, S., Champion, E., Bernache-Assollant, D., and Thomas, P. (2002) Calcium phosphate apatites with variable Ca/P atomic ratio I. Synthesis, characterisation and thermal stability of powders. Biomaterials, 23(4), 1065-1072.

Rey, C., Beshah, K., Griffin, R., and Glimcher, M.J. (1991a) Structural studies of the mineral phase of calcifying cartilage. Journal of Bone and Mineral Research, 6(5), 515-525.

Rey, C., Collins, B., Goehl, T., Dickson, I.R., and Glimcher, M.J. (1989a) The carbonate environment in bone mineral – A resolution-enhanced Fourier-transform infrared spectroscopy study. Calcified Tissue International, 45(3), 157-164.

Rey, C., Combes, C., Drouet, C., Lebugle, A., Sfihi, H., Barroug, A. (2007a) Nanocrystalline apatites in biological systems: characterisation, structure and properties. Materialwissenschaft und Werkstofftechnik, 38(12), 996-1002.

592 -. (2007b) Physico-chemical properties of nanocrystalline apatites: Implications for biominerals and
593 biomaterials. Materials Science and Engineering C, 27(2), 198-205.
594 Rey, C., Hina, A., Tofighi, A., and Glimcher, M.J. (1995) Maturation of poorly crystalline apatites: Chemical and
595 structural aspects in vivo and in vitro. Cells and Materials, 5(4), 345-356.
596 Rey, C., Lian, J., Grynpas, M., Shapiro, F., Zylberberg, L., and Glimcher, M.J. (1989b) Non-apatitic environments
597 in bone mineral: FT-IR detection, biological properties and changes in several disease states.
598 Connective tissue research, 21(1-4), 267-73.
599 Rey, C., Renugopalakrishnan, V., Collins, B., and Glimcher, M.J. (1991b) Fourier-transform infrared spectroscopy
600 study of the carbonate ions in bone mineral during aging. Calcified Tissue International, 49(4), 251-258.
601 Rey, C., Shimizu, M., Collins, B., and Glimcher, M.J. (1990) Resolution-enhanced Fourier-transform infrared
602 spectroscopy study of the environment of phosphate ions in the early deposits of a solid phase of
603 calcium phosphate in bone and enamel, and their evolution with age. 1. Investigations in the ν_4 PO_4
604 domain. Calcified Tissue International, 46(6), 384-394.
605 Robie, R.A., and Hemingway, B.S. (1995) U.S. Geological Survey Bull., 2131.
606 Roufosse, A.H., Aue, W.P., Roberts, J.E., Glimcher, M.J., and Griffin, R.G. (1984) Investigation of the mineral
607 phases of bone by solid-state P-31 magic angle sample spinning nuclear magnetic-resonance.
608 Biochemistry, 23(25), 6115-6120.
609 Sakhno, Y., Bertinetti, L., Iafisco, M., Tampieri, A., Roveri, N., and Martra, G. (2010) Surface Hydration and
610 Cationic Sites of Nanohydroxyapatites with Amorphous or Crystalline Surfaces: A Comparative Study.
611 Journal of Physical Chemistry C, 114(39), 16640-16648.
612 Ushakov, S.V., Helean, K.B., Navrotsky, A., and Boatner, L.A. (2001) Thermochemistry of rare-earth
613 orthophosphates. Journal of Materials Research, 16(9), 2623-2633.
614 Vandecandelaere, N., Rey, C., and Drouet, C. (2012) Biomimetic apatite-based biomaterials: on the critical
615 impact of synthesis and post-synthesis parameters. Journal of Materials Science-Materials in Medicine,
616 23(11), 2593-2606.

617 Vogel, W., and Hosemann, R. (1970) Evaluation of paracrystalline distortions from line broadening. Acta
618 Crystallographica Section A, 26(2), 272-277.
619 Wagman, D.D., Evans, W.H., Parker, V.B., Schumm, R.H., Halow, I., Bailey, S.M., Churney, K.L., and Nuttall, R.L.
620 (1982) The NBS tables of chemical thermodynamic properties – Selected values for inorganic and C-1
621 and C-2 organic substances in SI units. Journal of Physical and Chemical Reference Data, 11, 1-&.
622 Weiner S and Wagner HD. (1998) The material bone: Structure mechanical function relations. Ann. Rev. Mater.
623 Sci., 28, 271-298.
624 Winand, L. (1961) Etude physico-chimique du phosphate tricalcique hydrate et de l'hydroxylapatite. Ann Chim
625 (Paris), 13th series, 6, 941-967.
626 Wu, Y.T., Ackerman, J.L., Kim, H.M., Rey, C., Barroug, A., and Glimcher, M.J. (2002) Nuclear magnetic
627 resonance spin-spin relaxation of the crystals of bone, dental enamel, and synthetic hydroxyapatites.
628 Journal of Bone and Mineral Research, 17(3), 472-480.

629
630
631
632

Figure captions:

Figure 1: TEM micrograph for a biomimetic apatite sample matured for 1 day

Figure 2: XRD pattern for nanocrystalline apatite samples with varying maturation times

Figure 3: a) FTIR spectrum for a nanocrystalline apatite sample matured 1 day, b) detail in the □4PO4 vibration region for a sample matured 1 week

Figure 4: a) Evolution of $\Delta H_f°$ and $\Delta G_f°$ for nanocrystalline apatites versus maturation time in solution (uncertainties are two standard deviations, SD, of the mean), and b) linear fit for $\Delta H_f° = f(Ca^{2+}$ content)

Figure 5: Evolution of $\Delta G_{maturation}(i \rightarrow f)$ versus maturation time, taking the 20-min-matured sample as initial state

Table captions:

Table 1: Chemical composition of apatite samples (estimated uncertainty on each ion content: 0.5%)

Table 2: Thermodynamic cycle used in the calculations of $\Delta H_{f,oxides}$ and $\Delta H_f°$

Table 3: Experimental ΔH_{ds} values and derived $\Delta H_{f,oxides}$ and $\Delta H_f°$ for nanocrystalline apatites and for reference compounds HA and β-TCP

Table 4: Evaluation of $S°$, $\Delta S_f°$ and $\Delta G_f°$ for nanocrystalline apatites matured between 20 min and 3 weeks and for stoichiometric HA

668 Figure 1: TEM micrograph for a biomimetic apatite sample matured for 1 day

669

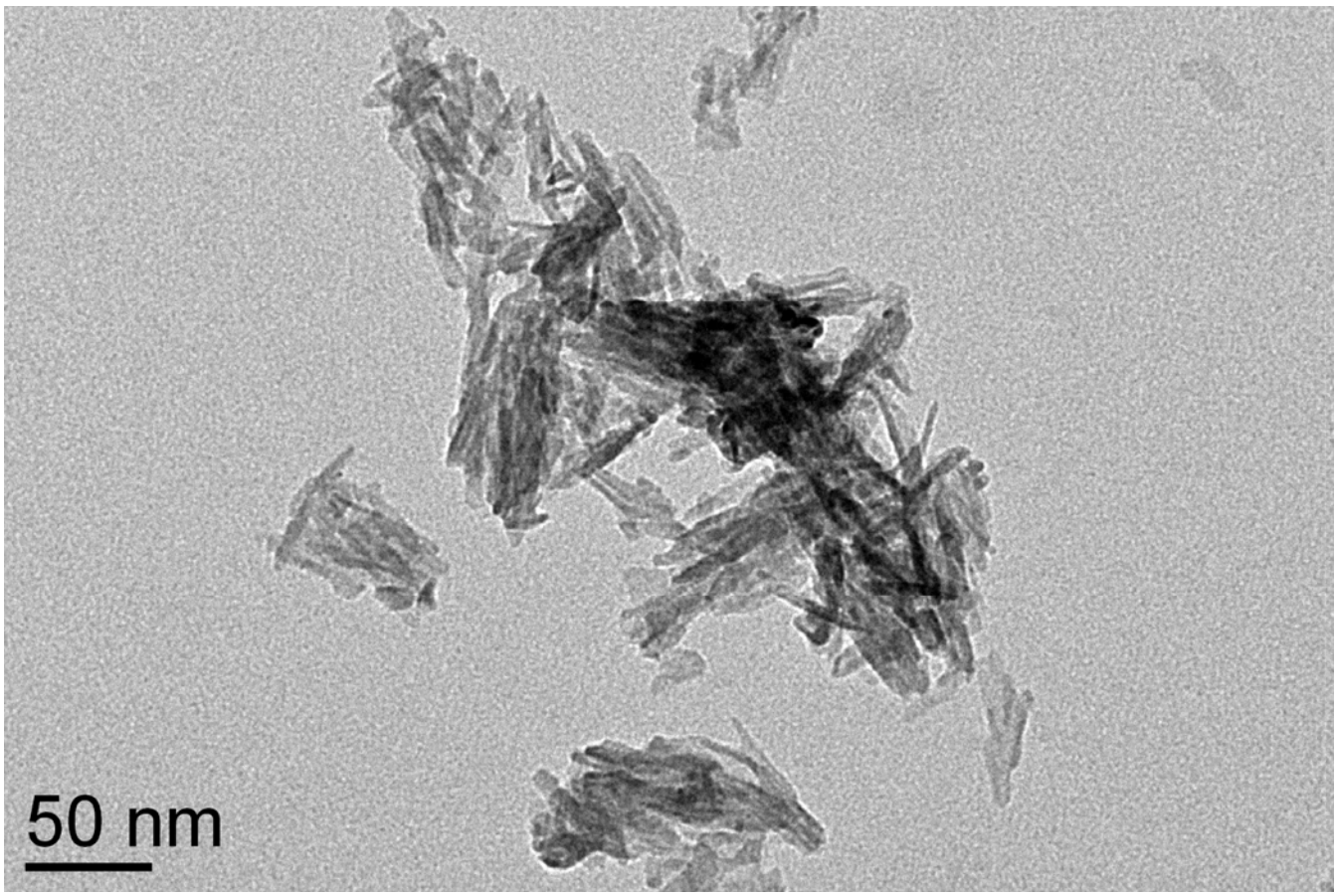

670

671

672

673 Figure 2: XRD pattern for nanocrystalline apatite samples with varying maturation times

674

675

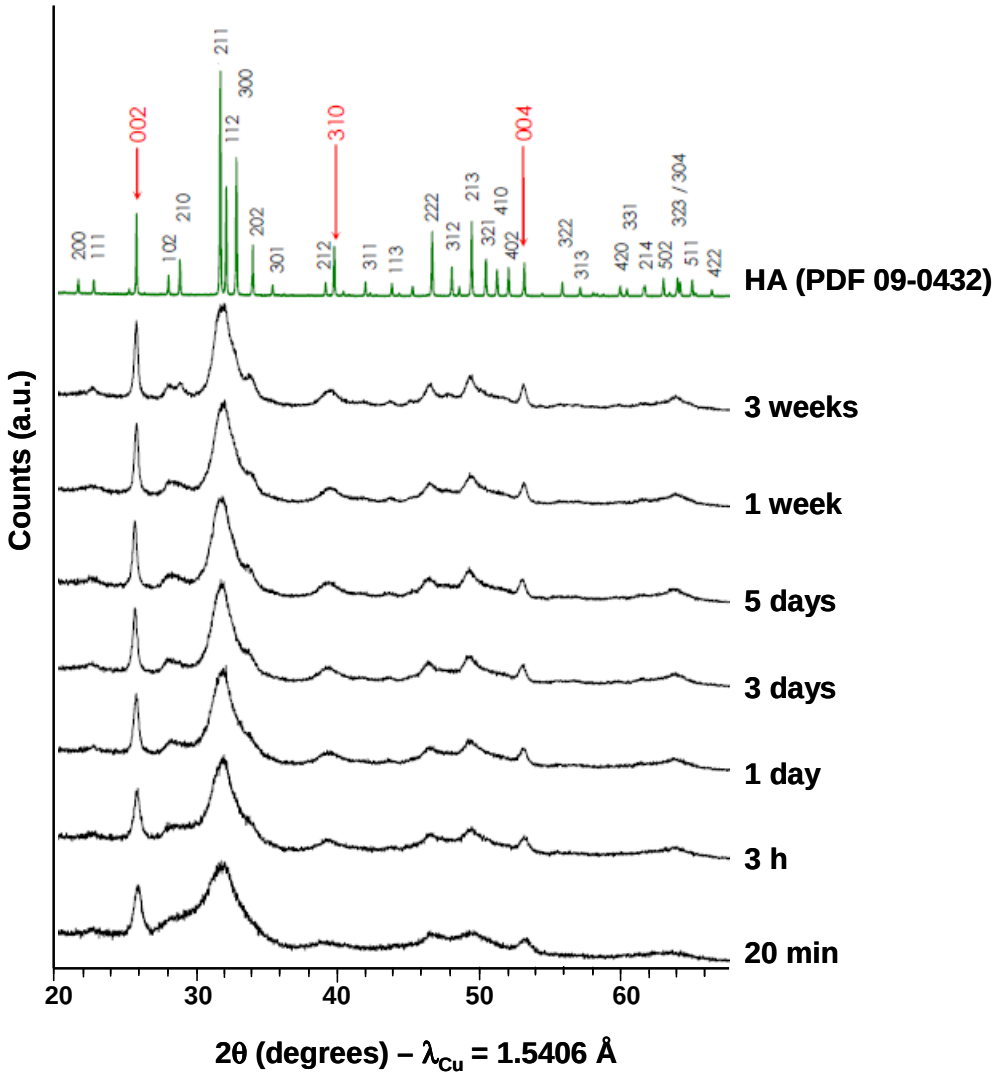

676

677

678

679

Figure 3: a) FTIR spectrum for a nanocrystalline apatite sample matured 1 day, b) detail in the ν_4PO_4 vibration region for a sample matured 1 week

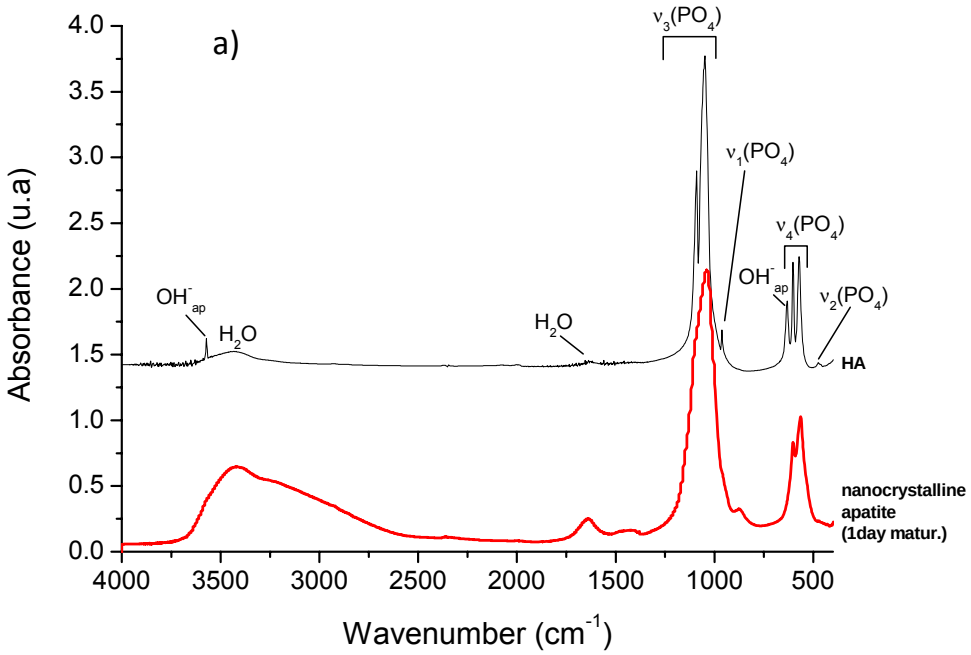

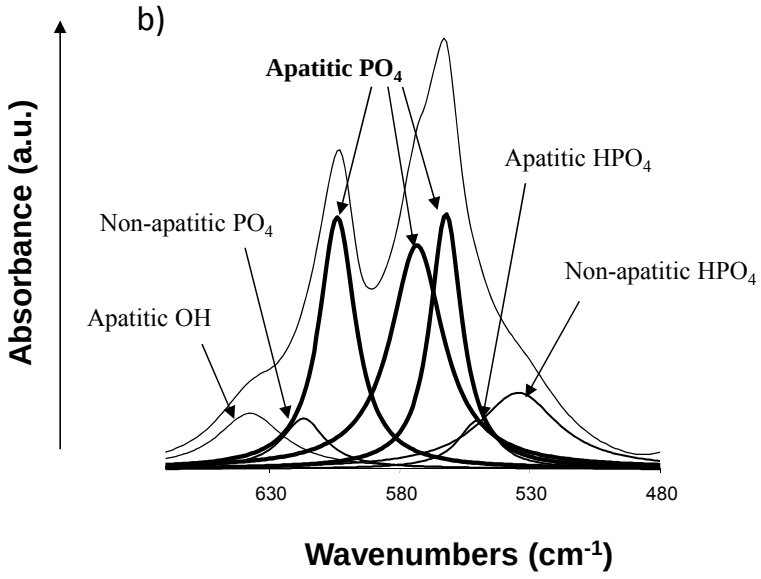

689 Figure 4: a) Evolution of $\Delta H_f°$ and $\Delta G_f°$ for nanocrystalline apatites versus maturation time in solution (uncertainties are two standard
690 deviations, SD, of the mean), and b) linear fit for $\Delta H_f°$ = f(Ca^{2+} content)

691

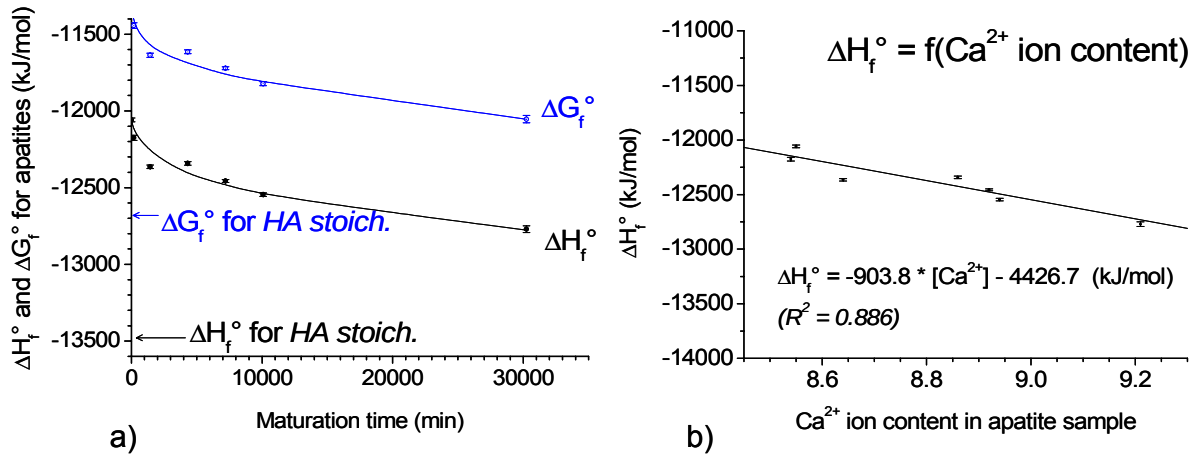

692
693
694
695
696

697 Figure 5: Evolution of $\Delta G_{maturation}$(i→f) versus maturation time, taking the 20-min-matured sample as initial state (± SD)

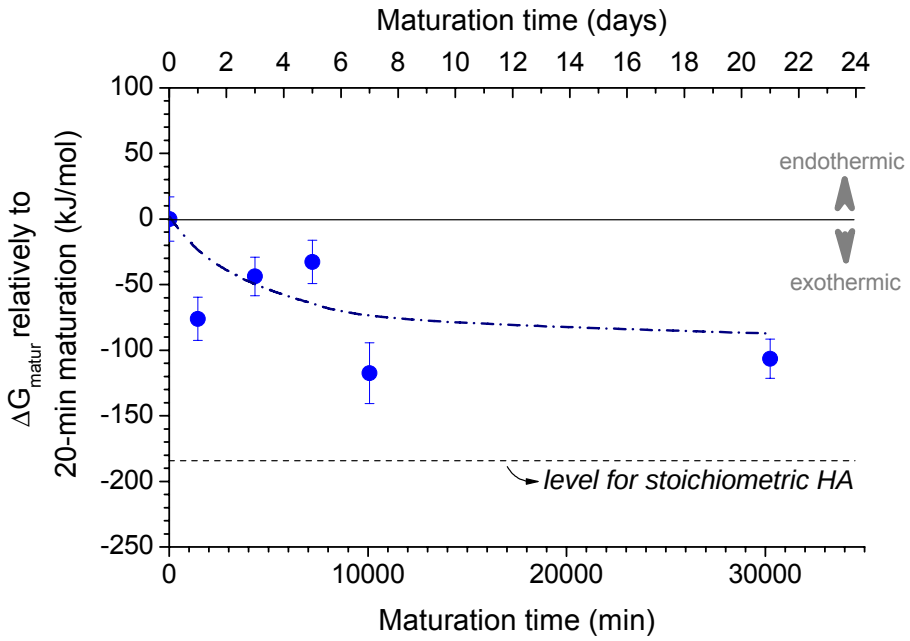

698

699 Table 1: Chemical composition of apatite samples (estimated uncertainty on each ion content: 0.5%)

700

Maturation time	Ca/P mole ratio	Value of Z *	Contents (moles per apatite unit formula *)				
			Ca^{2+}	PO_4^{3-}	HPO_4^{2-}	OH^-	H_2O
20 min	*1.43*	0.42	8.55	4.97	1.03	0.13	5.94
3 h	*1.42*	0.43	8.54	4.97	1.03	0.12	4.18
1 d	*1.44*	0.24	8.64	4.88	1.12	0.39	3.60
3 d	*1.48*	0.39	8.86	5.25	0.75	0.46	3.53
5 d	*1.49*	0.12	8.92	5.04	0.96	0.80	3.21
1 wk	*1.49*	0.17	8.94	5.11	0.89	0.77	2.86
3 wk	*1.54*	0.07	9.21	5.28	0.72	1.15	3.28

701 * considering Kühl and Nebergall's expression $Ca_{10-x-Z}(PO_4)_{6-x}(HPO_4)_x(OH)_{2-x-2Z}$

702

703

704

705 Table 2: Thermodynamic cycle used in the calculations of $\Delta H_f°$

706

Reactions:		ΔH
(1)	$Ca_{10-x-Z}(PO_4)_{6-x}(HPO_4)_x(OH)_{2-x-2Z}(H_2O)_n \rightarrow$ (10-x-Z) CaO (soln, 973) + 3 P_2O_5 (soln, 973) +(1-Z+n) H_2O (g, 973)	ΔH_{ds}(apatite, hydrated)
	Reactions from oxides:	
(2)	$CaCO_3$ (s, 298) $\rightarrow$ CaO (soln, 973) + CO_2 (g, 973)	$\Delta H_{ds}(CaCO_3)$
(3)	CO_2 (g, 298) $\rightarrow$ CO_2 (g, 973)	$\Delta H_{hc}(CO_2$ (g))
(4)	P_2O_5 (s, 298) $\rightarrow$ P_2O_5 (soln, 973)	$\Delta H_{ds}(P_2O_5)$
(5)	H_2O (g, 298) $\rightarrow$ H_2O (g, 973)	$\Delta H_{hc}(H_2O(g))$
(6)	H_2O (l, 298) $\rightarrow$ H_2O (g, 298)	$\Delta H°_{vap,\ 298}(H_2O(l))$
	Reactions from elements:	
(7)	Ca (s, 298) + C (s, 298) + 3/2 O_2 (g, 298) $\rightarrow$ $CaCO_3$ (s, 298)	$\Delta H_f°(CaCO_3)$
(8)	C (s, 298) + O_2 (g, 298) $\rightarrow$ CO_2 (g, 298)	$\Delta H_f°(CO_2$ (g))
(9)	Ca (s, 298) + 1/2 O_2 (g, 298) $\rightarrow$ CaO (s, 298)	$\Delta H_f°(CaO)$
(10)	2 P (s, 298) + 5/2 O_2 (g, 298) $\rightarrow$ P_2O_5 (s, 298)	$\Delta H_f°(P_2O_5)$
(11)	H_2 (g, 298) + ½ O_2 (g, 298) $\rightarrow$ H_2O (g, 298)	$\Delta H_f°(H_2O(g))$
Formation of nanocrystalline apatites from the oxides:		
(12)	(10-x-Z) CaO (s, 298) + 3 P_2O_5 (s, 298) + (2-x-2Z+n) H_2O (l, 298) $\rightarrow$ $Ca_{10-x-Z}(PO_4)_{6-x}(HPO_4)_x(OH)_{2-x-2Z}(H_2O)_n$	$\Delta H_{f,\ oxides}°$ (apatite)
Therefore:		
$\Delta H_{f,\ oxides}°$ (apatite) = $-\Delta H_1 + (10-x-Z)\ \Delta H_{ds}(CaO) + 3\ \Delta H_4 + (2-x-2Z+n)\ \Delta H_5 + (2-x-2Z+n)\ \Delta H_6$		
	$= -\Delta H_1 + (10-x-Z)\ [\Delta H_2 + \Delta H_7 - \Delta H_9 - \Delta H_8 - \Delta H_3] + 3\ \Delta H_4 + (2-x-2Z+n)\ \Delta H_5 + (2-x-2Z+n)\ \Delta H_6$	
Formation of nanocrystalline apatites from the elements:		
(13)	(10-x-Z) Ca (s, 298) + 6 P (s, 298) + (1-Z+n) H_2 (g, 298) + (26-x-2Z+n)/2 O_2 (g, 298) $\rightarrow$ $Ca_{10-x-Z}(PO_4)_{6-x}(HPO_4)_x(OH)_{2-x-2Z}(H_2O)_n$	$\Delta H_f°$ (apatite, hydrated)
Therefore :		
$\Delta H_f°$ (apatite, hydrated) = $-\Delta H_1 + (10-x-Z)\ \Delta H_2 + (10-x-Z)\ \Delta H_7 - (10-x-Z)\ \Delta H_3 - (10-x-Z)\ \Delta H_8 + 3\ \Delta H_4 + 3\ \Delta H_{10} + (1-Z+n)\ \Delta H_5 + (1-Z+n)\ \Delta H_{11}$		
	$\cong \Delta H_f°$ (apatite, anhydrous) + n $\Delta H_f°(H_2O(l))$	

707

708

709

710

711 Table 3: Experimental ΔH_{ds} values and derived $\Delta H_{f,oxides}$ and $\Delta H_f°$ for nanocrystalline apatites and for reference compounds HA and β-
712 TCP (± SD)

713

Sample	ΔH_{ds} (kJ/mol)	$\Delta H_f°$ (compound) (kJ/mol)	298 K, 1 atm	
Reference compounds:				
β-TCP	267.3 ± 9.7 (6)*	-4090.2 ± 10.6		
HA stoich.	1027.7 ± 21.4 (11)	-13431.0 ± 22.7		
Sample	**ΔH_{ds} (kJ/mol)**	**$\Delta H_f°$ (apatite, hydrated) (kJ/mol)**	**$\Delta H_{f\ oxides}$ (kJ/mol)**	**$\Delta H_f°$ (kJ/mol)**
Nanocrystalline apatites:				
20 min	1197.7 ± 10.0 (10)	-13756.8 ± 12.2	-1952.2 ± 12.5	-12058.9 ± 12.2
3 hour	1198.2 ± 15.0 (9)	-13370.7 ± 16.5	-2073.9 ± 16.8	-12174.9 ± 16.5
1 day	1241.7 ± 9.5 (8)	-13393.4 ± 11.8	-2152.7 ± 12.1	-12364.4 ± 11.8
3 days	1088.6 ± 9.1 (9)	-13352.3 ± 11.5	-2032.8 ± 11.8	-12342.1 ± 11.5
5 days	1077.4 ± 5.1 (9)	-13373.3 ± 8.7	-2030.5 ± 9.2	-12457.0 ± 8.7
1 week	1137.2 ± 9.1 (10)	-13362.2 ± 11.5	-2119.5 ± 11.9	-12546.1 ± 11.5
3 weeks	1172.8 ± 20.2 (9)	-13708.7 ± 21.4	-2141.3 ± 21.6	-12771.0 ± 21.4

* numbers in parentheses indicate the number of drop solution calorimetry experiments

714

715

716

717

718

719 Table 4: Evaluation of S°, $\Delta S_f°$ and $\Delta G_f°$ for nanocrystalline apatites matured between 20 min and 3 weeks, and for stoichiometric HA (±
720 SD)

721

722

723

724

Sample	At 298 K			
	Estimated S° J/(mol.K) [± 20 J/(mol.K)]	Estimated $\Delta S°_f$ J/(mol.K) [± 20 J/(mol.K)]	Recall of $\Delta H°_f$ kJ/mol	Corresponding $\Delta G°_f$ kJ/mol
Nanocrystalline apatite compounds:				
20 min	*695.2*	*-2 469*	-12 058.9 ± 12.2	-11 323.1 ± 12.2
3 hour	*694.6*	*-2 467*	-12 174.9 ± 16.5	-11 439.7 ± 16.5
1 day	*706.6*	*-2 512*	-12 364.4 ± 11.8	-11 616.0 ± 11.8
3 days	*708.2*	*-2 507*	-12 342.1 ± 11.5	-11 595.0 ± 11.5
5 days	*722.9*	*-2 565*	-12 457.0 ± 8.7	-11 692.6 ± 8.7
1 week	*721.4*	*-2 558*	-12 546.1 ± 11.5	-11 783.9 ± 11.5
3 weeks	*736.5*	*-2 607*	-12 771.0 ± 21.4	-11 994.2 ± 21.4
Stoichiometric HA	*769.5*	*-2 704*	-13 477 ± 10	-12 674.2 ± 10

725

726

727

Supplementary files as **Additional Resources for the Review process**:

Figure AR1: TG analysis on nanocrystalline apatite. Graph: example for 20-min maturation time. Inlet: evolutions of weight losses Δm_1, Δm_2 and Δm_3 (as described below) versus maturation (SEM on Δm_1: 0.01%, SEM on Δm_2 and Δm_3: 0.1%)

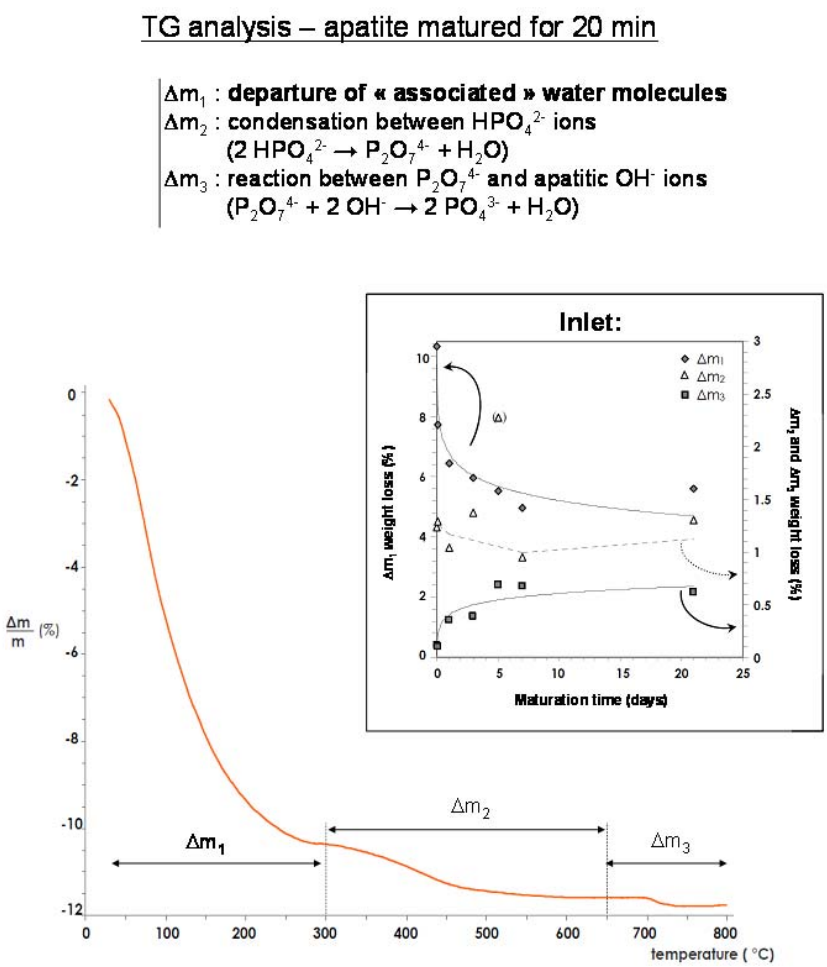

738 **Figure AR2: Plot of Ca^{2+} and OH^- ion contents (± SEM) per apatite unit formula, versus maturation time**

739

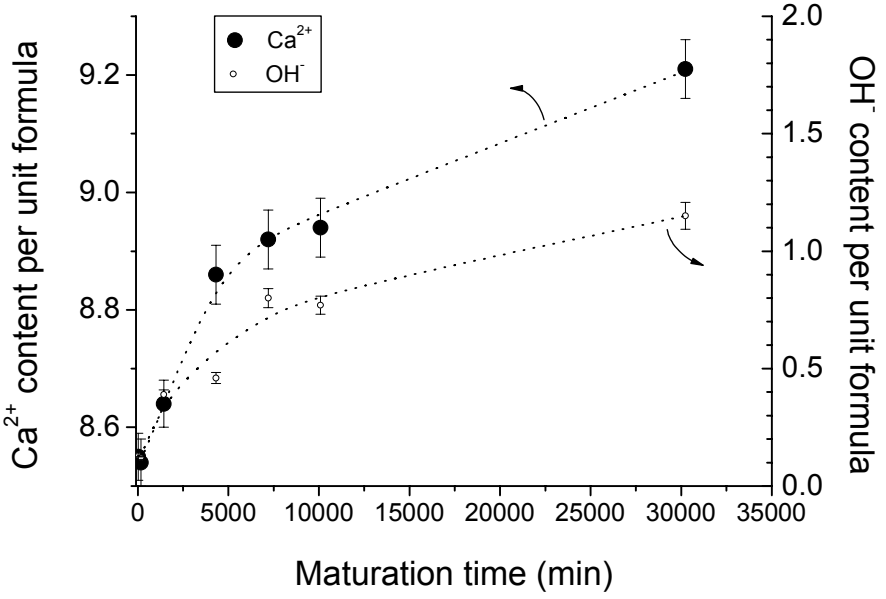

740

741 **Figure AR3: Plots of $\Delta H_f°$ versus Ca^{2+} (plot a) and OH^- (plot b) ion content in apatite, and of $\Delta G_f°$ versus Ca^{2+} (plot c), and**
742 **related linear fits**

743

a)

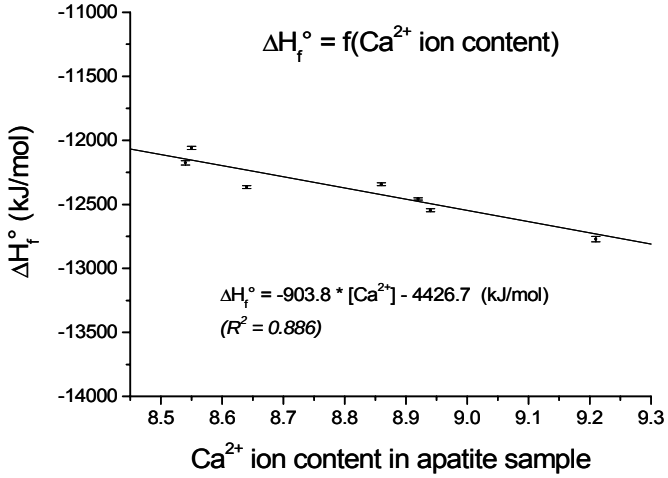

b)

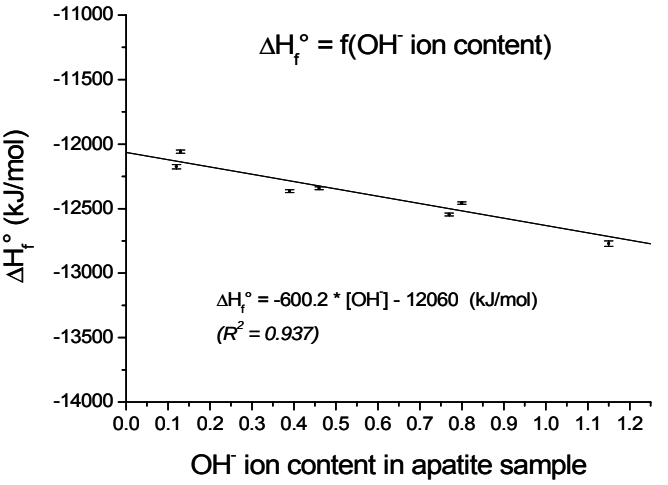

c)

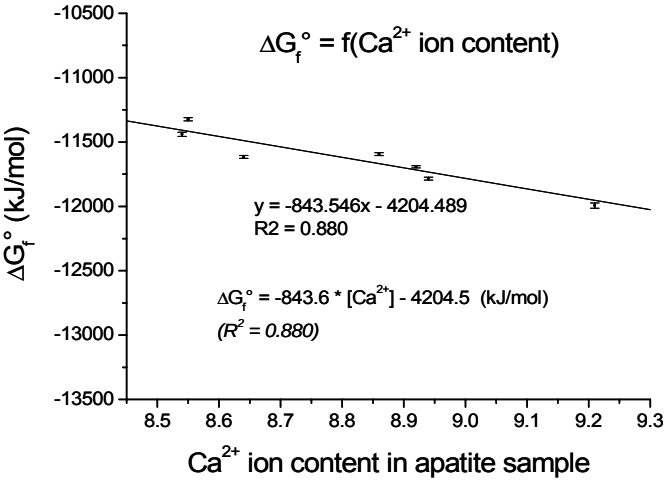

744
745
746
747

Figure AR4: Thermodynamic literature data for stoichiometric hydroxy-, fluor- and chlor-apatites (after Jemal et al. 1995; Jemal 2004; Ben Cherifa et al. 2004)

	$\Delta G_f°_{298}$ (kJ/mol)	$\Delta H_f°_{298}$ (kJ/mol)	$\Delta S_f°_{298}$ (kJ/(mol.K))
hydroxyapatites			
$Ca_{10}(PO_4)_6(OH)_2$	-12 674	-13 477	-2.69
$Sr_{10}(PO_4)_6(OH)_2$	-12 587	-13 373	-2.64
$Pb_{10}(PO_4)_6(OH)_2$	-7482	-8 261	-2.61
$Cd_{10}(PO_4)_6(OH)_2$	-7 873	-8 652	-2.61
$Ba_{10}(PO_4)_6(OH)_2$	-12 553	-13 309	-2.54
fluorapatites			
$Ca_{10}(PO_4)_6F_2$	-12 781	-13 558	-2.61
$Cd_{10}(PO_4)_6F_2$	-8 045	-8 795	-2.52
$Sr_{10}(PO_4)_6F_2$	-12 845	-13 604	-2.55
$Pb_{10}(PO_4)_6F_2$	-7 782	-8 529	-2.51
$Ba_{10}(PO_4)_6F_2$	-12 834	-13 564	-2.45
chlorapatites			
$Ca_{10}(PO_4)_6Cl_2$	-12 418	-13 180	-2.56
$Cd_{10}(PO_4)_6Cl_2$	-7 719	-8 463	-2.50
$Sr_{10}(PO_4)_6Cl_2$	-12 478	-13 233	-2.53
$Pb_{10}(PO_4)_6Cl_2$	-7 458	-8 220	-2.56
$Ba_{10}(PO_4)_6Cl_2$	-12 418	-13 246	-2.78

760

761 **Figure AR5: Estimation of theoretical solubility products (at 298 K) for nanocrystalline apatites matured for varying periods of**
762 **time, as drawn from $\Delta G°_{disso}$ calculation**

763

764

765

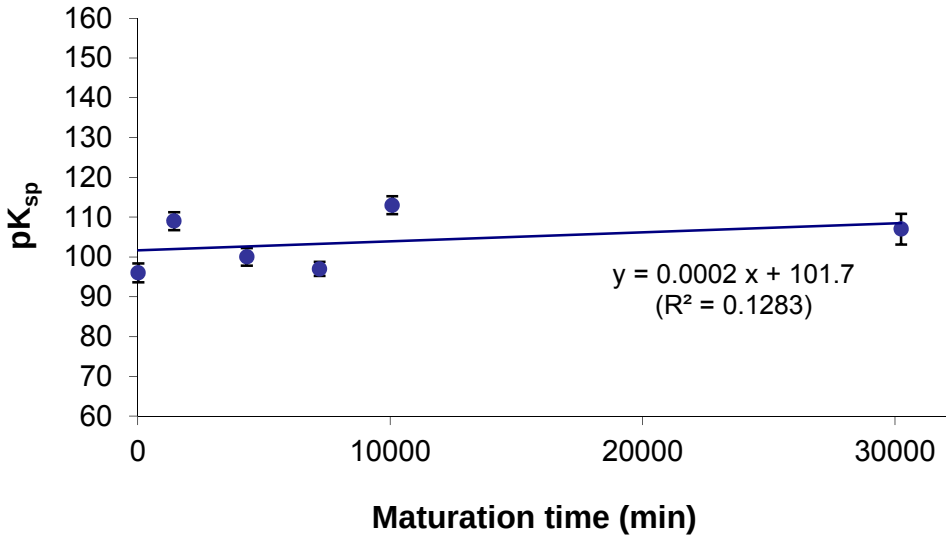

766

767

768